Supporting Information

Co/Fe_3O_4 Nanoparticles Embedded in N-doped Hierarchical Porous Carbon Derived from Zeolitic Imidazolate Frameworks as Efficient Oxygen Reduction Electrocatalysts for Zinc-Air Battery-based Desalination

Jinhong Dai[1], Jingzhe Zhang[1], R. Karthick[1], Mengjun Liang[1], Qiang Wei[1], Xuncai Chen[2], Yumeng Shi[3], Shengli Zhai[1,5*], Guannan Wang[4*], Fuming Chen[1,5*]*

[1] *Guangdong Provincial Key Laboratory of Quantum Engineering and Quantum Materials, Guangdong Engineering Technology Research Center of Efficient Green Energy and Environment Protection Materials, School of Physics and Telecommunication Engineering, South China Normal University, Guangzhou 510006, P.R. China.*

[2] *Guangzhou Key Laboratory of Forensic Multi-Omics for Precision Identification, School of Forensic Medicine, Southern Medical University, Guangzhou 510515, China.* xche3815@smu.edu.cn

[3] *College of Electronics and Information Engineering, Shenzhen University, Shenzhen 518060, China.*

[4] *College of Medical Engineering& the Key Laboratory for Medical Functional Nanomaterials, Jining Medical University, Jining 272067, China. chemwangguannan@gmail.com*

[5] *School of Electronics and Information Engineering, South China Normal University, Foshan, 528225, China. victor_zsl@163.com; fmchen@m.scnu.edu.cn*

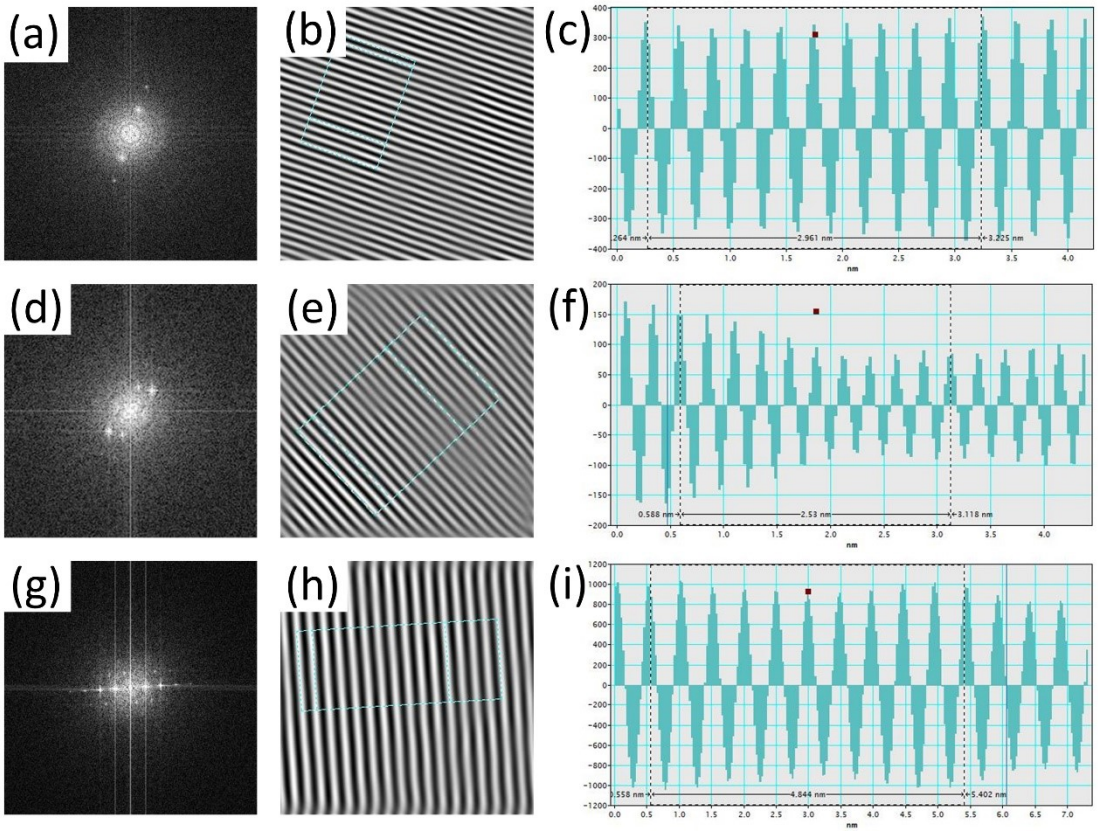

Fig. S1 The profiles of (a, d, g) fast fourier transform (FFT), (b, e, h) inverse fast fourier transform (IFFT) and (c, f, i) calculation related to (220), (311) and (111) planes of Fe_3O_4 in Fig. 4e.

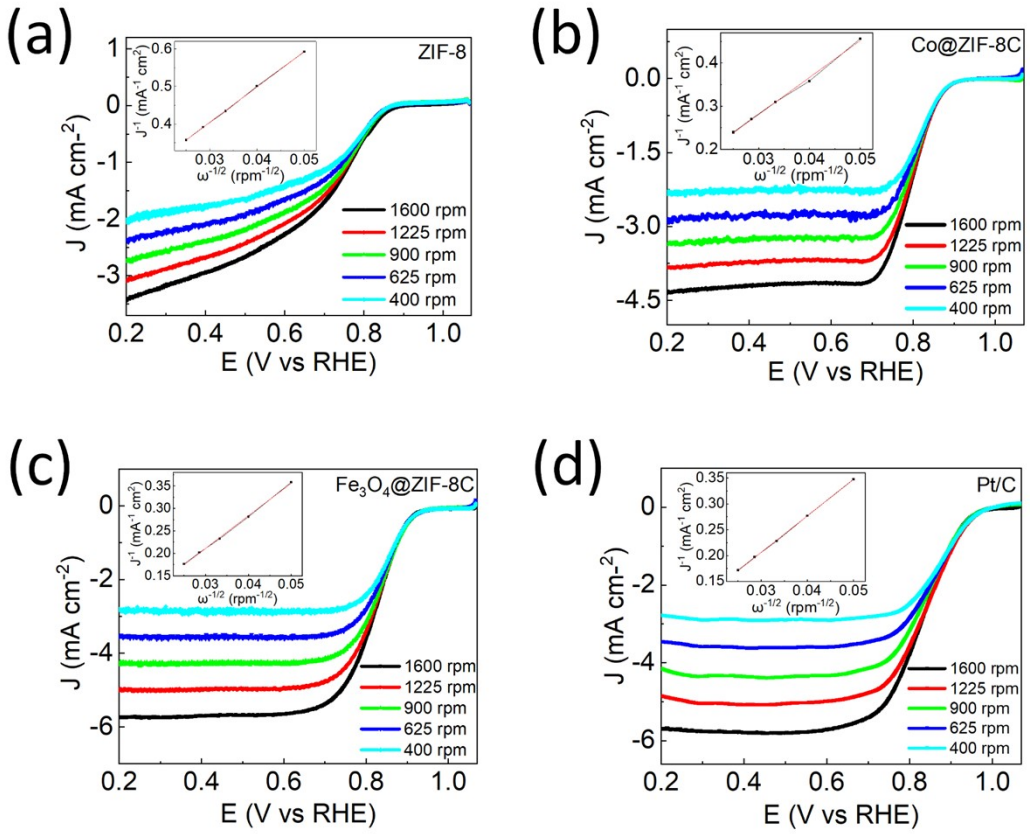

Fig. S2 (a-d) LSV curves of ORR on ZIF-8C, Co@ZIF-8C, Fe_3O_4@ZIF-8C and commercial Pt/C at different rotation rates (from 400 to 1600 rpm).

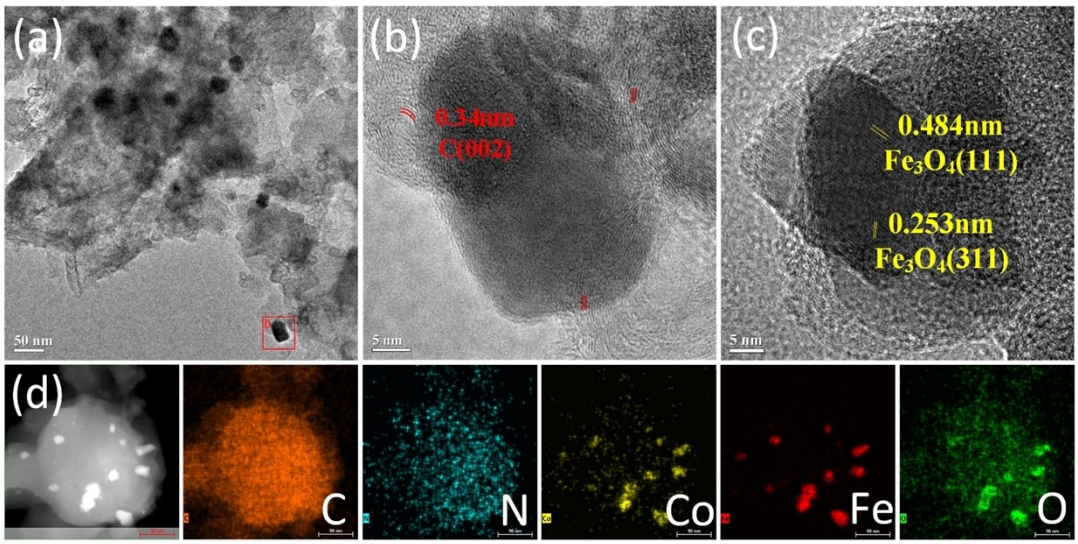

Fig. S3 (a-c) TEM images with different magnifications. (d) HAADF-STEM picture and corresponding EDS mapping images of Co/Fe_3O_4@ZIF-8C sample after 30,000 seconds of stability test.

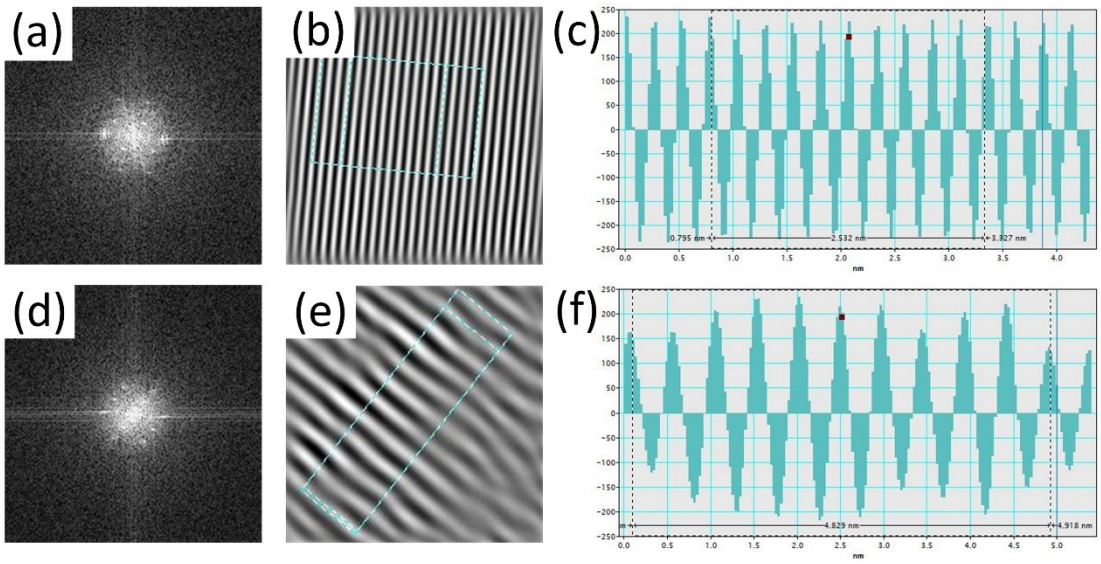

Fig. S4 The profiles of (a, d) fast fourier transform (FFT), (b, e) inverse fast fourier transform (IFFT) and (c, f) calculation related to (311) and (111) planes of Fe_3O_4 in Fig. S3c.

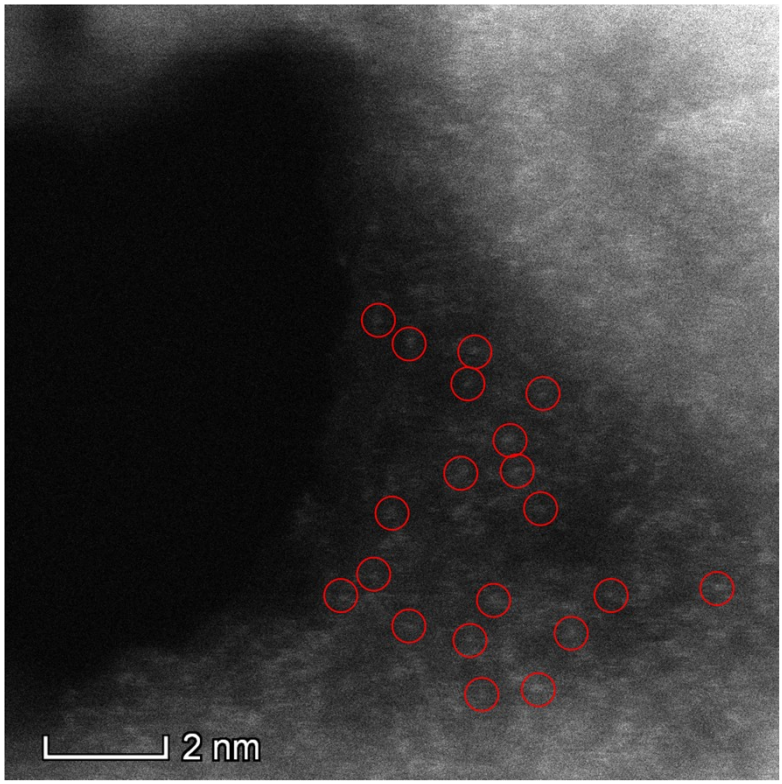

Fig. S5 Dark-field high-resolution TEM image showing highly dispersed Co atoms in carbon layers.

As for the composition effect on the ORR activity of Co/Fe_3O_4@ZIF-8C, a series of samples with different molar ratios (4:1, 3:2, 2:3 and 1:4) of precursors $CoCl_2 \cdot 6H_2O$ to $FeCl_3 \cdot 6H_2O$ were investigated. As depicted in **Fig. S6-7** and **Table S4**, the ratio of 1:4 not only manifests the largest limiting current density, electron transfer number and the smallest tafel slope, but also presents the most positive oxygen reduction peak, onset potential as well as half-wave potential relative to other ratios. These results reflect that the amount of Co/ Fe_3O_4 nanoparticles embedded into the ZIF-8-derived carbon makes a significant sense of ORR performance. More importantly, the Co/Fe_3O_4@ZIF-8C (specifically denotes the ratio of 1:4) sample was measured to have optimal electrocatalytic activity among these four ratios.

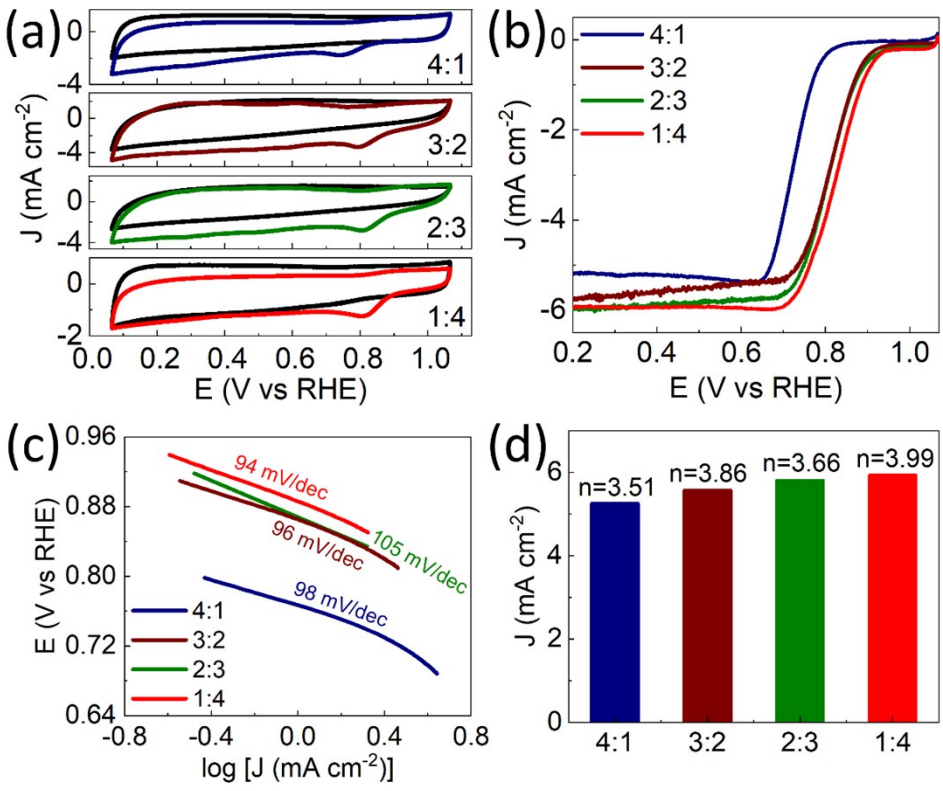

Fig. S6 (a) CV curves of four Co/Fe_3O_4@ZIF-8C catalysts with different molar ratios of Co to Fe in N_2- (black lines) and O_2-saturated (colored lines) 0.1 M KOH electrolyte at a scan rate of 50 mV s^{-1}. (b) LSV curves of ORR on Co/Fe_3O_4@ZIF-8C catalysts with different molar ratios of Co to Fe in O_2-saturated 0.1 M KOH electrolyte at a scan rate of 10 mV s^{-1} and a rotation rate of 1600 rpm. (c) Tafel plots of four studied materials. (d) Current density (J) and the corresponding electron-transfer number (n) of ORR on different materials at around 0.46 V (vs RHE).

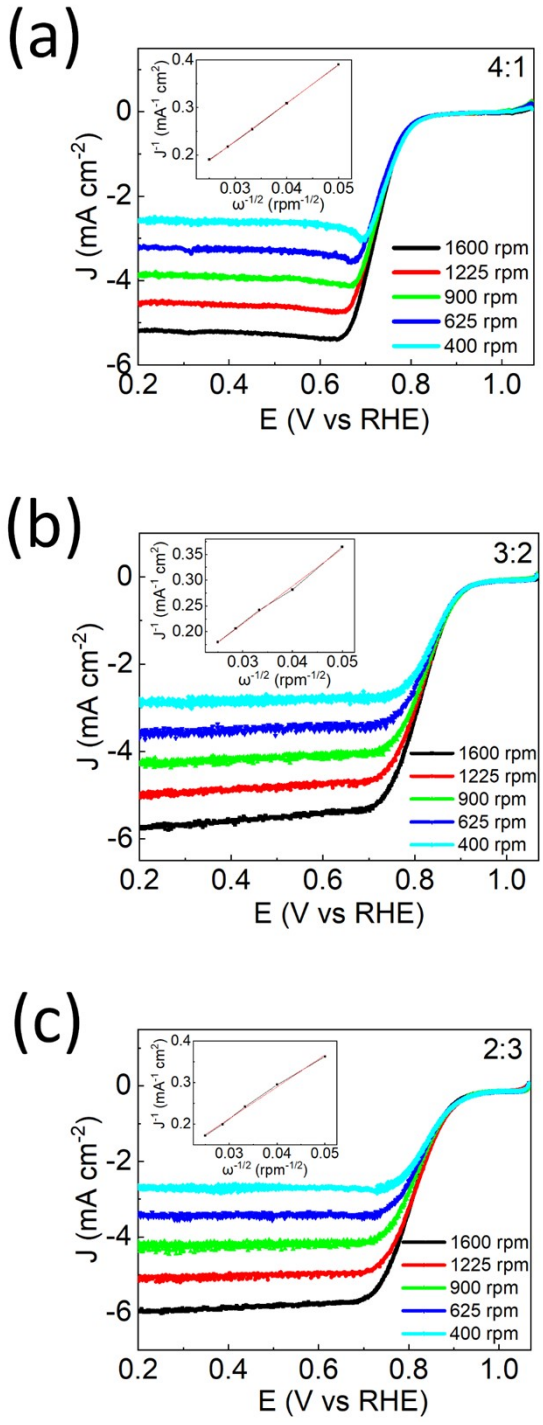

Fig. S7 (a-c) LSV curves of ORR on Co/Fe_3O_4@ZIF-8C catalysts at different rotation rates (from 400 to 1600 rpm) when the molar ratios of Co to Fe are 4:1, 3:2, and 2:3, respectively.

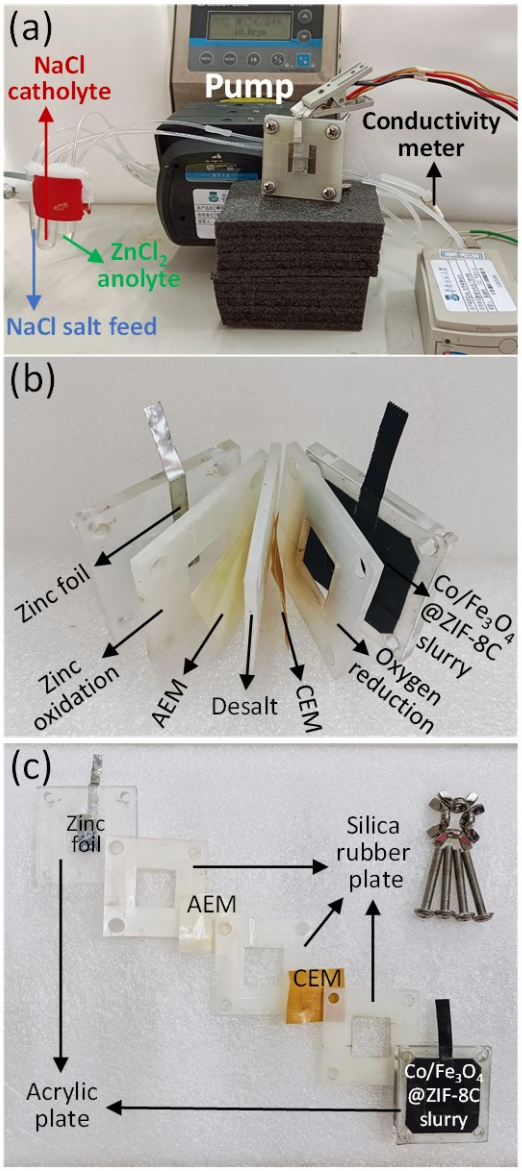

Fig. S8 The photographs of (a) the whole ZABD device and (b-c) the separate battery components with Co/Fe_3O_4@ZIF-8C as the cathode catalyst. The ZABD device was assembled in the sequence as shown in (b-c).

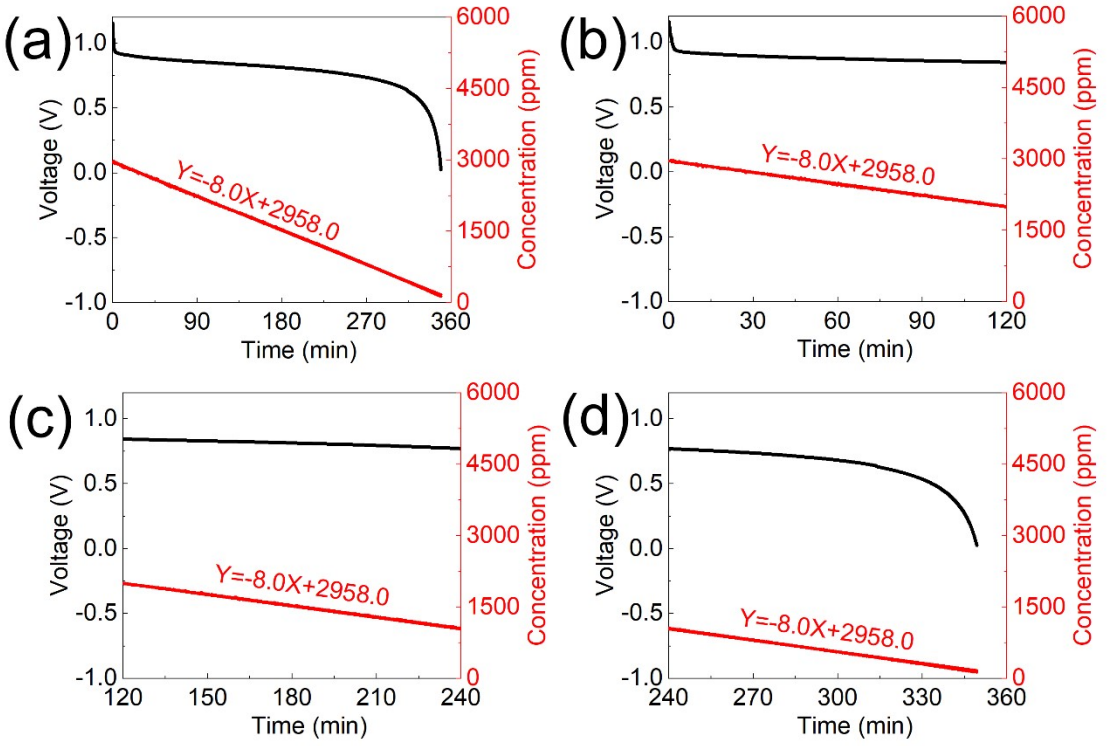

Fig. S9 (a) The continuous electrochemical performance of Zn-air battery-based desalination with Co/Fe_3O_4@ZIF-8C as the cathode catalyst at a current density of 1.0 mA cm^{-2} during the discharging-desalination process over 300 min, (b-d) the zoom-in sections at different periods.

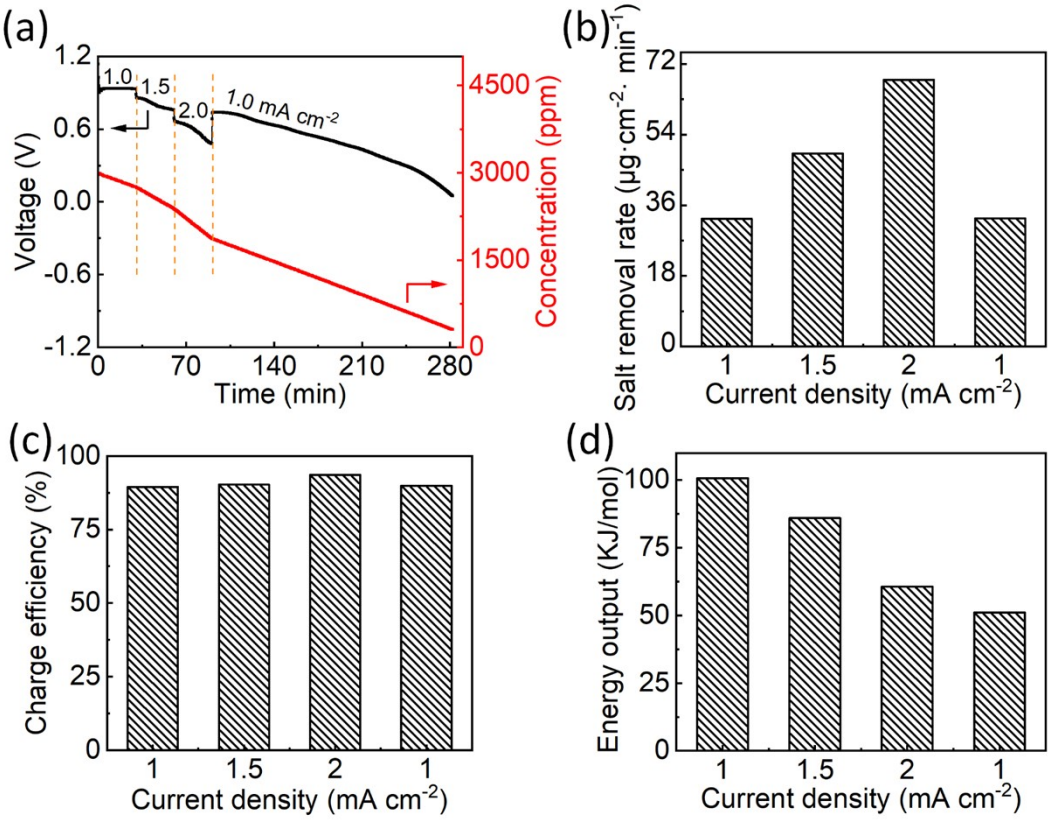

Fig. S10 (a) Changes in voltage and salt feed concentration under various discharge current densities. The corresponding desalination performances of salt removal rate (b), charge efficiency (c), and energy output (d) at each current density.

Table S1 The textural parameters of ZIF-8C, Co@ZIF-8C, Fe_3O_4@ZIF-8C and Co/Fe_3O_4@ZIF-8C.

Electrocatalyst	BET specific surface area (m^2 g^{-1})	Total pore volume (cm^3 g^{-1})	Average pore size (nm)
ZIF-8C	1005.3	0.574	2.284
Co@ZIF-8C	510.6	0.351	2.747
Fe_3O_4@ZIF-8C	597.7	0.655	4.381
Co/Fe_3O_4@ZIF-8C	663.1	0.709	4.277

Table S2 Electrochemical properties of ZIF-8C, Co@ZIF-8C, Fe_3O_4@ZIF-8C, Co/Fe_3O_4@ZIF-8C and Pt/C in O_2-saturated 0.1 M KOH electrolyte.

Electrocatalyst	Onset potential (V vs RHE)	Half-wave potential (V vs RHE)	Limiting current density (mA cm^{-2})
ZIF-8C	0.85	0.73	2.79
Co@ZIF-8C	0.88	0.80	4.17
Fe_3O_4@ZIF-8C	0.91	0.82	5.68
Co/Fe_3O_4@ZIF-8C	0.93	0.83	5.93
Pt/C	0.94	0.83	5.82

In this work, the measured current density at 0.46 V (vs RHE) is uniformly taken as the limiting current density, and the potentials at half and 5 % of the limiting current density are taken as the half-wave potential and onset potential, respectively.

Table S3 Comparison of the ORR performance of the sample in this work with other reported electrocatalysts in 0.1 M KOH electrolyte.

Electrocatalyst	O_2 reduction peak (V vs RHE)	Onset potential (V vs RHE)	Limiting current density (mA cm^{-2})	Electron transfer number	Ref.
Co/Fe_3O_4@ZIF-8C	0.81	0.93	5.93	3.99	This work
NP-C-800	0.78	0.90	4.79	3.86	[1]
GOBN5-750	<0.7	0.798	3.0	3.7	[2]
FeNCSs	0.86	0.96	~	3.86-3.99	[3]
Fe_3C-Co/NC	0.83	0.94	5.5	3.9	[4]
Fe_3O_4@NC/NHPC	~	0.898	4.77	3.91	[5]
Fe_3O_4@FeNC	~	1.007	~6	3.96	[6]
FeCo/FeCoNi@NCNTs-HF	0.834	~	5.775	3.98-4.00	[7]
Co@G/N-GCNs	~	0.95	~	3.96	[8]
Co/Co_4N@N-CNT/rGO	~0.8	~	4.82	~4.0	[9]
N,P-HCS	0.71	0.880	5.62	3.95	[10]

Table S4 Electrochemical properties of four Co/Fe_3O_4@ZIF-8C catalysts with different molar ratios of Co to Fe in O_2-saturated 0.1 M KOH electrolyte.

Molar ratio of Co to Fe in Co/Fe_3O_4@ZIF-8C electrocatalyst	Onset potential (V vs RHE)	Half-wave potential (V vs RHE)	Limiting current density (mA cm^{-2})
4:1	0.81	0.73	5.25
3:2	0.91	0.81	5.57
2:3	0.93	0.81	5.81
1:4	0.93	0.83	5.93

Table S5 Performance comparison of Zinc-Air battery-based desalination with Co/Fe_3O_4@ZIF-8C and Pt/C applied to cathode catalyst respectively.

Electrocatalyst	Salt removal rate ($\mu g\ cm^{-2}\ min^{-1}$)	Charge efficiency (%)	Energy output ($KJ\ mol^{-1}$)
Co/Fe_3O_4@ZIF-8C	32.9	90.5	91.6
Pt/C	33.7	92.7	73.4

Parameter Calculation

Potential vs. Reversible Hydrogen Electrode (E_{RHE}, V):

$$E_{RHE} = E_{Hg/HgO} + 0.059PH + E^{0}_{Hg/HgO}$$

Where $E_{Hg/HgO}$ is the measured potential against Hg/HgO reference electrode during the test, $E^{0}_{Hg/HgO}$ is the standard electrode potential of Hg/HgO (0.098 V).

Koutechy-Levich (K-L) equation:

$$\frac{1}{J} = \frac{1}{J_L} + \frac{1}{J_K} = \frac{1}{B\omega^{1/2}} + \frac{1}{J_K}$$

$$B = 0.62nFD^{2/3}\upsilon^{-1/6}C$$

Where J is the measured current density (A cm^{-2}), J_L and J_K are the diffusion-limiting and kinetic-limiting current densities (A cm^{-2}), respectively, ω is the angular velocity (rad s^{-1}) of the disk, F is the Faraday constant (96485 C mol^{-1}), D is the diffusion coefficient of oxygen in 0.1 M KOH electrolyte (1.9×10^{-5} cm^2 s^{-1}), ν is the kinetic viscosity of electrolyte (0.01 cm^2 s^{-1}), and C is the concentration of dissolved oxygen in 0.1 M KOH solution (1.2×10^{-6} mol cm^{-3}).

Salt removal rate (*v, μg cm^{-2} min^{-1}*)：

$$\nu = (\frac{\Delta c}{\Delta t} \times V)/A$$

Where Δc/Δt is the salt concentration change per minute (Δppm min^{-1}), V is the volume of the salt stream (mL), and A is the active electrode area (*i.e.*, 1 cm^2 for the exposed zinc foil).

Charge efficiency *(Γ, %)* is defined as the percentage of salt removals to the total electrons used:

$$\Gamma = \frac{(\frac{\Delta c \times 10^{-3}}{\Delta t} \times T \times \frac{V \times 10^{-3}}{M_{NaCl}})}{\frac{I \times T \times 60}{F}} \times 100\%$$

where Δc/Δt is the salt concentration change per minute (Δppm min^{-1}), T is the desalination time (min), V is the volume of the salt stream (mL), M_{NaCl} is the molar mass of NaCl (58.44 g mol^{-1}), I is the current intensity (A), and F is the Faraday constant (96485 C mol^{-1}).

Energy output ($\bar{E}$, *kJ* mol^{-1}) describes the average energy released when one mole of salt is removed during the discharge-desalination process:

$$\bar{E} = \frac{\int_0^{T \times 60} UIdt \times 10^{-3}}{(\frac{\Delta c \times 10^{-3}}{\Delta t} \times T \times \frac{V \times 10^{-3}}{M_{NaCl}})}$$

where U is the monitored instant voltage of desalination battery (V), I is the current intensity (A), T is the desalination time (min), Δc/Δt is the salt concentration change per minute (Δppm min^{-1}), V is the volume of the salt stream (mL), and M_{NaCl} is the molar mass of NaCl (58.44 g mol^{-1}).

References:

1. X. Chen, L. Wei, Y. Wang, S. Zhai, Z. Chen, S. Tan, Z. Zhou, A. K. Ng, X. Liao and Y. Chen, *Energy Storage Mater.*, 2018, **11**, 134-143.

2. I. M. Patil, M. Lokanathan and B. Kakade, *J. Mater. Chem. A*, 2016, **4**, 4506-4515.

3. T. Zhou, Y. Zhou, R. Ma, Q. Liu, Y. Zhu and J. Wang, *J. Mater. Chem. A*, 2017, **5**, 12243-12251.

4. C. C. Yang, S. F. Zai, Y. T. Zhou, L. Du and Q. Jiang, *Adv. Funct. Mater.*, 2019, **29**, 1901949.

5. Y. Wang, M. Wu, K. Wang, J. Chen, T. Yu and S. Song, *Adv. Sci.*, 2020, **7**, 2000407.

6. S. Hu, W. Ni, D. Yang, C. Ma, J. Zhang, J. Duan, Y. Gao and S. Zhang, *Carbon*, 2020, **162**, 245-255.

7. Z. Wang, J. Ang, B. Zhang, Y. Zhang, X. Y. D. Ma, T. Yan, J. Liu, B. Che, Y. Huang and X. Lu, *Appl. Catal. B: Environ.*, 2019, **254**, 26-36.

8. H. J. Niu, L. Zhang, J. J. Feng, Q. L. Zhang, H. Huang and A. J. Wang, *J. Colloid Interface Sci.*, 2019, **552**, 744-751.

9. H. Qi, Y. Feng, Z. Chi, Y. Cui, M. Wang, J. Liu, Z. Guo, L. Wang and S. Feng, *Nanoscale*, 2019, **11**, 21943-21952.

10. C. Zhang, L. Hou, C. Cheng, Z. Zhuang, F. Zheng and W. Chen, *ChemElectroChem*, 2018, **5**, 1891-1898.